

Dear Author,

Here are the proofs of your article.

- You can submit your corrections **online**, via **e-mail** or by **fax**.
- For **online** submission please insert your corrections in the online correction form. Always indicate the line number to which the correction refers.
- You can also insert your corrections in the proof PDF and **email** the annotated PDF.
- For fax submission, please ensure that your corrections are clearly legible. Use a fine black pen and write the correction in the margin, not too close to the edge of the page.
- Remember to note the **journal title**, **article number**, and **your name** when sending your response via e-mail or fax.
- **Check** the metadata sheet to make sure that the header information, especially author names and the corresponding affiliations are correctly shown.
- **Check** the questions that may have arisen during copy editing and insert your answers/ corrections.
- **Check** that the text is complete and that all figures, tables and their legends are included. Also check the accuracy of special characters, equations, and electronic supplementary material if applicable. If necessary refer to the *Edited manuscript*.
- The publication of inaccurate data such as dosages and units can have serious consequences. Please take particular care that all such details are correct.
- Please **do not** make changes that involve only matters of style. We have generally introduced forms that follow the journal's style. Substantial changes in content, e.g., new results, corrected values, title and authorship are not allowed without the approval of the responsible editor. In such a case, please contact the Editorial Office and return his/her consent together with the proof.
- If we do not receive your corrections **within 48 hours**, we will send you a reminder.
- Your article will be published **Online First** approximately one week after receipt of your corrected proofs. This is the **official first publication** citable with the DOI. **Further changes are, therefore, not possible.**
- The **printed version** will follow in a forthcoming issue.

Please note

After online publication, subscribers (personal/institutional) to this journal will have access to the complete article via the DOI using the URL: [http://dx.doi.org/\[DOI\]](http://dx.doi.org/[DOI]).

If you would like to know when your article has been published online, take advantage of our free alert service. For registration and further information go to: <http://www.link.springer.com>.

Due to the electronic nature of the procedure, the manuscript and the original figures will only be returned to you on special request. When you return your corrections, please inform us if you would like to have these documents returned.

Metadata of the article that will be visualized in OnlineFirst

ArticleTitle	Modeling and Simulating Depositional Sequences Using Latent Gaussian Random Fields	
Article Sub-Title		
Article CopyRight	International Association for Mathematical Geosciences (This will be the copyright line in the final PDF)	
Journal Name	Mathematical Geosciences	
Corresponding Author	Family Name	Allard
	Particle	
	Given Name	Denis
	Suffix	
	Division	
	Organization	INRAE, BioSP
	Address	84914, Avignon, France
	Phone	
	Fax	
	Email	denis.allard@inrae.fr
	URL	
	ORCID	http://orcid.org/0000-0001-7944-1906
Author	Family Name	Fabbri
	Particle	
	Given Name	Paolo
	Suffix	
	Division	
	Organization	University of Padua
	Address	Padua, Italy
	Phone	
	Fax	
	Email	paolo.fabbri@unipd.it
	URL	
	ORCID	
Author	Family Name	Gaetan
	Particle	
	Given Name	Carlo
	Suffix	
	Division	
	Organization	Ca' Foscari University of Venice
	Address	Venice, Italy
	Phone	
	Fax	
	Email	gaetan@unive.it
	URL	

ORCID

Schedule	Received	17 February 2020
	Revised	
	Accepted	21 May 2020

Abstract	<p>Simulating a depositional (or stratigraphic) sequence conditionally on borehole data is a long-standing problem in hydrogeology and in petroleum geostatistics. This paper presents a new rule-based approach for simulating depositional sequences of surfaces conditionally on lithofacies thickness data. The thickness of each layer is modeled by a transformed latent Gaussian random field allowing for null thickness thanks to a truncation process. Layers are sequentially stacked above each other following the regional stratigraphic sequence. By choosing adequately the variograms of these random fields, the simulated surfaces separating two layers can be continuous and smooth. Borehole information is often incomplete in the sense that it does not provide direct information about the exact layer that some observed thickness belongs to. The latent Gaussian model proposed in this paper offers a natural solution to this problem by means of a Bayesian setting with a Markov chain Monte Carlo (MCMC) algorithm that can explore all possible configurations that are compatible with the data. The model and the associated MCMC algorithm are validated on synthetic data and then applied to a subsoil in the Venetian Plain with a moderately dense network of cored boreholes.</p>
----------	---

Keywords (separated by '-')	Subsoil modeling - Stratigraphic sequence - PC prior - Stochastic 3D model - Data augmentation - Conditional simulation
-----------------------------	---

Footnote Information	
----------------------	--



Modeling and Simulating Depositional Sequences Using Latent Gaussian Random Fields

Denis Allard¹ · Paolo Fabbri² · Carlo Gaetan³

Received: 17 February 2020 / Accepted: 21 May 2020
© International Association for Mathematical Geosciences 2020

1 **Abstract** Simulating a depositional (or stratigraphic) sequence conditionally on bore-
2 hole data is a long-standing problem in hydrogeology and in petroleum geostatistics.
3 This paper presents a new rule-based approach for simulating depositional sequences
4 of surfaces conditionally on lithofacies thickness data. The thickness of each layer is
5 modeled by a transformed latent Gaussian random field allowing for null thickness
6 thanks to a truncation process. Layers are sequentially stacked above each other fol-
7 lowing the regional stratigraphic sequence. By choosing adequately the variograms of
8 these random fields, the simulated surfaces separating two layers can be continuous
9 and smooth. Borehole information is often incomplete in the sense that it does not
10 provide direct information about the exact layer that some observed thickness belongs
11 to. The latent Gaussian model proposed in this paper offers a natural solution to this
12 problem by means of a Bayesian setting with a Markov chain Monte Carlo (MCMC)
13 algorithm that can explore all possible configurations that are compatible with the
14 data. The model and the associated MCMC algorithm are validated on synthetic data
15 and then applied to a subsoil in the Venetian Plain with a moderately dense network
16 of cored boreholes.

1

2

✉ Denis Allard
denis.allard@inrae.fr

Paolo Fabbri
paolo.fabbri@unipd.it

Carlo Gaetan
gaetan@unive.it

¹ INRAE, BioSP, 84914 Avignon, France

² University of Padua, Padua, Italy

³ Ca' Foscari University of Venice, Venice, Italy

17 **Keywords** Subsoil modeling · Stratigraphic sequence · PC prior · Stochastic 3D
18 model · Data augmentation · Conditional simulation

19 **1 Introduction**

20 The case study motivating this work is a subsoil in the Venetian Plain with a moderately
21 dense network of cored boreholes. Geologists and hydrogeologists managing this sub-
22 soil are in need of stochastic three-dimensional models of the stratigraphic sequence.
23 The model should of course be conditioned to borehole data. The sequence of layers
24 must correspond to the known regional stratigraphic sequence and, in addition, to the
25 surfaces separating the layers are required to be smooth and continuous.

26 Simulating a depositional (or stratigraphic) sequence conditionally on boreholes
27 data has been and still is a long-standing problem in hydrogeology and in petroleum
28 geostatistics. In the context of reservoir modeling, Pycrz et al. (2015) offers a compre-
29 hensive overview of the literature and a convincing conceptual framework in which
30 methods are represented along a complexity gradient with one extreme corresponding
31 to pixel based models with statistics and conditioning derived from the data and the
32 other extreme representing geological concepts unconditional to local observations.
33 As models tend to move away from the less complex extreme to the more complex
34 one, they are less versatile and more difficult to condition (Pycrz et al. 2015). Easy-to-
35 condition pixel based methods thus tend to be favored when data are dense, whereas
36 rule-based or process-based models are preferred when conditioning data is sparse.

37 Pixel based approaches, whether based on variograms (Matheron et al. 1987), trun-
38 cated Gaussian random fields and plurigaussian random fields (Beucher et al. 1993;
39 Galli et al. 1994; Armstrong et al. 2011; Le Blévec et al. 2017; Le Blévec et al.
40 2018), transiograms (Carle and Fogg 1996), or MCP (Allard et al. 2011; Sartore et al.
41 2016; Benoit et al. 2018b), are well known and relatively easy to handle. For these
42 approaches, variogram and transiogram fitting is well understood and conditioning to
43 well data is efficient, even for truncated Gaussian models (Marcotte and Allard 2018).
44 However, one source of difficulty in the fitting procedure is the fact that the processes
45 and the amount of information are often anisotropic. Typically, for borehole data, there
46 is much more information along the depth than along horizontal directions.

47 Multiple point statistics (MPS) approaches (Strebelle 2002; Mariethoz and Caers
48 2014) require a training image when simulations are performed in two dimensions.
49 Three-dimensional simulations are much more difficult to perform, since training
50 cubes are rarely available at kilometer scales. Methods for combining images in three-
51 dimensional simulations have been proposed (Comunian et al. 2012, 2014). But since
52 a high degree of continuity is required for layers in this work, pixel based methods,
53 including MPS, are not deemed appropriate.

54 Object models, such as Boolean models, are more difficult to fit and to condition,
55 in particular when accounting for non-stationarity and erosion rules, see for example
56 Syversveen and Omre (1997) and Allard et al. (2006). In addition, object models are
57 not geologically appropriate for simulating sequences of layers.

58 Rule-based and process-based models incorporate some amount of understanding of
59 the geological processes. They use rules to control the temporal sequence and spatial

60 position of geological objects so as to mimic geological processes. Among others,
61 they have been applied to fluvial systems, deepwater channel systems and turbiditic
62 lobes systems. Particular cases of interest to this work are surface-based models. For
63 simulating lobes in a turbidite reservoir, Bertoncello et al. (2013) proposed a rule-based
64 stacking of lobe-shape events with quite complicated sequential placement rules that
65 depend partly on the already simulated events. The conditioning to well-log data and
66 seismic data is achieved through sequential optimization. One of the limitations of this
67 approach is that the variability between the conditional simulations is low, owing to
68 the optimization approach. A second limitation recognized by the authors is that their
69 method works best with a limited amount of data.

70 This paper presents a new rule-based approach for simulating depositional
71 sequences of surfaces conditionally to lithofacies thickness data. It is a stochastic
72 model that belongs to the *Markov rules* sub-class of rule-based methods, see Pyrcz
73 et al. (2015) and appropriate references therein. The thickness of each layer is modeled
74 by a transformed latent Gaussian random field allowing for null thickness. The random
75 fields are *latent* because they can be unobserved on some parts of the domain under
76 study, thanks to a truncation process. Layers are sequentially stacked above each other
77 following the regional stratigraphic sequence. By choosing adequately the variograms
78 of these random fields, the simulated surfaces separating two layers can be continuous
79 and smooth. Conditioning to the observed borehole data is made possible thanks to
80 constrained Gaussian conditioning, as will be explained later on.

81 A problem that has been barely addressed in geostatistical models for depositional
82 sequences is the fact that borehole information is often incomplete in the sense that it
83 does not provide direct information regarding the exact layers that have been observed.
84 For example, let us consider that the stratigraphic sequence of the study domain con-
85 tains several repetitions of a given lithofacies, say Clay. Consider also that the recorded
86 data at one given borehole measures one single thickness for Clay. A first possibil-
87 ity is that there is actually only one Clay layer at this location, but it could be any
88 of the several Clay layers of the regional stratigraphic sequence. Simulations should
89 therefore account for this uncertainty. A second possibility is that the measurement
90 actually corresponds to two (or more) Clay layers, one on top of the other, with miss-
91 ing intermediate layers at this location. In this case, the measured thickness should be
92 shared between two layers. The latent Gaussian model proposed in this paper offers a
93 natural solution to this problem by means of a Bayesian setting with a Markov Chain
94 Monte Carlo (MCMC) algorithm that can explore all possible configurations compat-
95 ible with the data. Notice that the approach proposed in Bertoncello et al. (2013) does
96 not address this problem at all.

97 The rest of this paper is organized as follows. Section 2 is devoted to the concep-
98 tual model. In particular, the difference between the (unique) regional stratigraphic
99 sequence, referred to as the parent sequence, and the observed sequences is detailed.
100 Section 3 presents the stochastic model. In Sect. 4 all details for Bayesian inference
101 with an MCMC algorithm are given. It is then validated on a synthetic data set in
102 Sect. 5. Finally, it is successfully applied to the Venetian Plain that motivated this
103 work in Sect. 6. Some concluding remarks are then given in Sect. 7.

2 The Conceptual Model

2.1 Notations

Let us consider a spatial domain $\mathcal{S} \in \mathbb{R}^2$ and an interval $\mathcal{T} \subset \mathbb{R}^+$, which will correspond to “depth”. Note that depth can be converted into time through depositional processes, which is the reason why $t \in \mathcal{T}$ is used to denote depth. Let us also consider a family of K lithofacies, $\mathcal{C} = \{C_1, \dots, C_K\}$. The aim of this work is to build a process $X = \{X(s, t)\}$, defined at any point $(s, t) \in \mathcal{S} \times \mathcal{T}$ and taking values in \mathcal{C} . In other words, at each location is associated one and only one lithofacies. The process must be continuous almost everywhere and the discontinuity surfaces should be smooth and have a general horizontal orientation. The process X is observed along depth at a finite number of locations s_1, \dots, s_n and each observation corresponds to a drilled core, referred to as boreholes in the rest of this work.

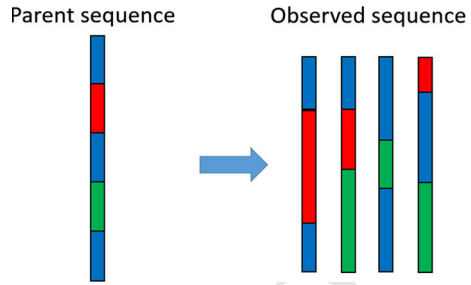
Let $X_i = \{X(s_i, t), t \in \mathcal{T}\}$ be one of these observations at site s_i , $i = 1, \dots, n$, where n is the number of sites. The observation X_i is piece-wise constant, with M_i discontinuities at different depths each time a new layer is encountered. The resulting information is a sequence of facies and depths, referred to as the *observed sequence*, $(\mathbf{C}_i^o, \mathbf{T}_i^o)$, where $\mathbf{C}_i^o = (C_{1,i}^o, \dots, C_{M_i,i}^o)$ with $C_{j,i}^o \in \mathcal{C}$ for $j = 1, \dots, M_i$, and $\mathbf{T}_i^o = (T_{1,i}^o, \dots, T_{M_i,i}^o)$ with $T_{j,i}^o \in \mathcal{T}$ and $T_{1,i}^o < \dots < T_{M_i,i}^o$. The depths are measured with respect to a ground-level $T_{0,i}$. The thicknesses of each observed layer $\mathbf{Z}_i^o = (Z_{1,i}^o, \dots, Z_{M_i,i}^o)$ can be derived from the depths, with $Z_{j,i}^o = T_{j,i}^o - T_{j-1,i}^o$, $j = 1, \dots, M_i$. Finally, the last layer is assumed to be completely observed, that is the depth $Z_{M_i,i}^o$ is assumed to be not censored.

2.2 Parent Sequence

The working hypothesis is that there exists a common lithological sequence of facies, hereafter referred to as the “parent sequence,” which is compatible with all observed sequences in the area of study in the sense that each observed sequence can be obtained from the parent sequence by deleting some layers of the parent sequence.

This sequence can result from the prior knowledge of the scientists. Alternatively, it can be derived from the observed data. From a mathematical viewpoint, there always exists a parent sequence. For example, it can easily be obtained by simply stacking all observed sequences into a single sequence. Then, each observed sequence of layers is simply obtained by “deleting” all other observed sequences. Obviously, this parent sequence is of no modeling interest, but it is mathematically important since it provides a proof of the existence of this concept. In general, very long parent sequences are uninteresting from a modeling point of view. In accordance with a parsimony principle, one should seek the shortest possible parent sequences. Clearly, there is only a finite number of parent sequences of minimal length. Such parent sequences could be built using discrete optimization algorithms, or they could be provided by scientists, based on prior geological knowledge. Either way, how minimal parent sequences are obtained is a subject out of the scope of the present research, and this route is not pursued any longer.

Fig. 1 Parent sequence and four possible incomplete observed sequences. Since the parent sequence is conceptual, thicknesses are only meaningful in the observed sequences



From now on it will be considered that the parent sequence is known, and that it is one of the minimal length parent sequences. The parent sequence of length M will be denoted $\mathbf{C} = (C_1, \dots, C_M)$, $C_i \in \mathcal{C}$, with $M \geq \max\{K, M_1, \dots, M_n\}$.

2.3 From the Parent Sequence to the Observed Sequences

When analyzing sequences of lithofacies, it is quite common that some facies are unobserved at one or several boreholes. In order to allow for this, each observed sequence at each site s_i is therefore a subset of a complete sequence $(\mathbf{C}, \mathbf{T}_i)$ corresponding to the parent sequence. The corresponding vector of complete thickness is \mathbf{Z}_i , and, in contrast to the observed ones, some thickness $Z_{j,i} = T_{j,i} - T_{j-1,i}$, $j = 1, \dots, M$ can be equal to zero. In this case, the corresponding layer is unobserved at location s_i . When $M_i < M$, the sequence at s_i is an *incomplete sequence*, and \mathbf{C}_i^o is a subsequence of \mathbf{C} . The complete data will be denoted $\mathbf{X} = \{(\mathbf{C}, \mathbf{Z}_i), i = 1, \dots, n\}$ and $\mathbf{X}^o = \{(\mathbf{C}_i^o, \mathbf{Z}_i^o), i = 1, \dots, n\}$ will denote the observed data. In the following, $O(\cdot)$ will denote the mapping such that $\mathbf{X}^o = O(\mathbf{X})$. Figure 1 illustrates a parent sequence and four different possible observed sequences.

3 Statistical Setting

3.1 Stochastic Model

The stochastic model requires a univariate model for the marginal distribution of the thicknesses and a spatial model to account for the lateral continuity of the layers. Thicknesses are modeled using positive zero inflated random variables in order to account for the many 0s resulting from incomplete observed sequences. Among many possible models, latent truncated Gaussian models (Allcroft and Glasbey 2003; Baxevani and Lennartsson 2015; Benoit et al. 2018a), also referred to as Tobit models (Liu et al. 2019) in econometrics, are flexible models that easily allow geostatistical modeling. Spatial dependence among the thicknesses belonging to a same layer is introduced by means of a truncated Gaussian random field. More precisely, for $j = 1, \dots, M$, let $W_j(s)$, $s \in \mathcal{S}$ be a standardized Gaussian random field that, for simplicity, will be supposed stationary with covariance function $\text{cov}[W_j(s), W_j(s')] = \rho_j(s - s'; \xi_j)$, where ρ_j is a parametric correlation function and ξ_j the vector of associated parameters. The thickness field $\{Z_j(s), s \in \mathcal{S}\}$ is defined as

$$Z_j(s) = \varphi_j(W_j(s) - \tau_j) \quad \text{if } W_j(s) > \tau_j, \quad (1)$$

and $Z_j(s) = 0$ otherwise, where τ_j is a threshold and $\varphi_j(\cdot)$ is a continuous one-to-one mapping from \mathbb{R}_+ to \mathbb{R}_+ . The probability of positive thickness $\Pr(Z_j(s) > 0)$ will be denoted by p_j . With this construction, null thickness has a positive probability, since $\Pr(Z_j(s) = 0) = 1 - p_j = \Phi(\tau_j) > 0$, where $\Phi(\cdot)$ is the cumulative probability function of the standard Gaussian random variable. Parameters of the stochastic model can be expressed equivalently in terms of τ_j or p_j and in the sequel the second setting is chosen. One particular case that will be used later is to set $\varphi_j(x) = \mu_j x^{\beta_j}$, $x > 0$ with $\beta_j, \mu_j > 0$. When $\beta_j = 1$, one gets

$$E[Z_j(s)] = \mu_j \left(\frac{\phi(\tau_j)}{1 - \Phi(\tau_j)} - \tau_j \right), \quad (2)$$

and

$$\text{Var}[Z_j(s)] = \mu_j^2 \left[1 + \frac{\phi(\tau_j)}{1 - \Phi(\tau_j)} \left(\tau_j - \frac{\phi(\tau_j)}{1 - \Phi(\tau_j)} \right) \right], \quad (3)$$

where $\phi(\cdot)$ is the density function of the standard Gaussian random variable. When β_j is not an integer, the moments of $Z_j(s)$ involve hypergeometric functions and are not reported here. From Eqs. (2) and (3), it is clear that the expectation and standard deviation of the thickness of layer j are both proportional to the parameter μ_j . The covariance function ρ_j must be smooth enough in order to generate regular thicknesses. For example, choosing that ρ_j is twice differentiable at the origin leads to a mean-squared differentiable random field W_j and, as a consequence, to a mean-squared differentiable random field for the thicknesses since φ_j is continuous and locally finite boundaries of the non null thickness sets. The depth surfaces $\{T_j(s), s \in \mathcal{S}\}$ are then obtained by adding up the thickness fields. Starting from a fixed and known ground-floor $T_0 = \{T_0(s), s \in \mathcal{S}\}$ one sets

$$T_j(s) = T_{j-1}(s) + Z_j(s) = T_0(s) + \sum_{i=1}^j Z_i(s), \quad j = 1, \dots, M.$$

Finally, the random fields W_j are assumed to be independent, since they relate to independent depositional processes.

3.2 Complete Likelihood

Since layers are assumed to be independent, the complete likelihood factorizes into a product of M likelihoods

$$L(\theta; \mathbf{X}) = \prod_{j=1}^M L_j(\theta_j; Z_{j,1}, \dots, Z_{j,n}), \quad (4)$$

205 where $\theta_j = (p_j, \mu_j, \beta_j, \xi_j)$, $j = 1, \dots, M$ and $\theta = (\theta_1, \dots, \theta_M)$.

206 In the sequel $\phi_k(\cdot, \boldsymbol{\mu}, \boldsymbol{\Sigma})$ and $\Phi_k(\cdot, \boldsymbol{\mu}, \boldsymbol{\Sigma})$ denote the density and the cumulative
 207 distribution function of a k -multivariate Gaussian random variable with mean vector
 208 $\boldsymbol{\mu}$ and covariance matrix $\boldsymbol{\Sigma}$. Let us consider now a layer $j \in \{1, \dots, M\}$. For conven-
 209 nience, thicknesses and the corresponding locations are reordered such that the first
 210 n_j thicknesses $Z_{j,1}, \dots, Z_{j,n_j}$ correspond to the positive values and the remaining
 211 $\ell_j = n - n_j$ ones are 0. The complete-data likelihood of the single layer j is

$$212 L_j(\theta_j; Z_{j,1}, \dots, Z_{j,n}) = f_j(Z_{j,1}, \dots, Z_{j,n_j}; \theta_j) F_j(0, \dots, 0, |Z_{j,1}, \dots, Z_{j,n_j}; \theta_j). \quad (5)$$

214 The density $f_j(Z_{j,1}, \dots, Z_{j,n_j}; \theta_j)$ is given by

$$215 f(Z_{j,1}, \dots, Z_{j,n_j}; \theta) = \phi_{n_j}(W_{j,1}, \dots, W_{j,n_j}; \mathbf{0}, \boldsymbol{\Sigma}_j) \prod_{i=1}^{n_j} J_{\varphi_j^{-1}}(Z_{j,i}), \quad (6)$$

216 where $\boldsymbol{\Sigma}_j = \boldsymbol{\Sigma}_{n_j, n_j} = [\rho(s_i - s_k; \xi_j)]_{i,k=1, \dots, n_j}$, $W_{j,i} = \varphi_j^{-1}(Z_{j,i}) + \tau_j$, $i =$
 217 $1, \dots, n_j$, and $J_{\varphi_j^{-1}}(Z_{j,i})$ is the Jacobian of φ_j^{-1} computed at $Z_{j,i}$. The conditional
 218 probability $F_j(0, \dots, 0 | Z_{j,1}, \dots, Z_{j,n_j}; \theta)$ is given by

$$219 F_j(0, \dots, 0 | Z_{j,1}, \dots, Z_{j,n_j}; \theta) = \Phi_{\ell_j}(\tau_j, \dots, \tau_j; \mathbf{m}_j, \mathbf{V}_j), \quad (7)$$

220 where the mean vector \mathbf{m}_j and covariance matrix \mathbf{V}_j can be easily derived using the
 221 Kriging equations (Cressie 1993; Chilès and Delfiner 2012)

$$222 \mathbf{m}_j = \boldsymbol{\Sigma}_{\ell_j, n_j} \boldsymbol{\Sigma}_{n_j, n_j}^{-1} \mathbf{W}_{n_j}; \quad \mathbf{V}_j = \boldsymbol{\Sigma}_{\ell_j, \ell_j} - \boldsymbol{\Sigma}_{\ell_j, n_j} \boldsymbol{\Sigma}_{n_j, n_j}^{-1} \boldsymbol{\Sigma}_{n_j, \ell_j}, \quad (8)$$

223 with $\mathbf{W}_{n_j} = (W_{j,1}, \dots, W_{j,n_j})'$ and the matrices $\boldsymbol{\Sigma}_{\ell_j, n_j}$ and $\boldsymbol{\Sigma}_{\ell_j, \ell_j}$ being defined in
 224 similar ways as $\boldsymbol{\Sigma}_{n_j, n_j}$. To summarize, the complete data likelihood in (4) becomes

$$225 L(\theta; \mathbf{X}) = \prod_{j=1}^M L_j(\theta; Z_{j,1}, \dots, Z_{j,n})$$

$$226 = \prod_{j=1}^M \phi_{n_j}(W_{j,1}, \dots, W_{j,n_j}; \mathbf{0}, \boldsymbol{\Sigma}_j)$$

$$227 \times \prod_{i=1}^{n_j} J_{\varphi_j^{-1}}(Z_{j,i}) \Phi_{\ell_j}(\tau_j, \dots, \tau_j; \mathbf{m}_j, \mathbf{V}_j). \quad (9)$$

228 In the particular case $\varphi_j(x) = \mu_j x^{\beta_j}$ that will be considered below, the Jacobian
 229 simplifies to

$$230 \quad J_{\varphi_j^{-1}}(Z_{j,i}) = \frac{1}{\mu_j \beta_j} \left(\frac{Z_{j,i}}{\mu_j} \right)^{1-1/\beta_j}. \quad (10)$$

231 3.3 Observed Likelihood

232 In principle, the observed likelihood is related to the complete likelihood through

$$233 \quad L(\theta; \mathbf{X}^o) = \int_{\{\mathbf{X} : \mathbf{X}^o = O(\mathbf{X})\}} L_X(\theta; \mathbf{X}) d\mathbf{X}. \quad (11)$$

234 However, even for moderately long parent sequence and number of 0 thicknesses,
 235 the space $\{\mathbf{X} : \mathbf{X}^o = O(\mathbf{X})\}$ is difficult to explore and the integral (11) becomes
 236 intractable. These difficulties are illustrated with two examples. At some site, let us
 237 consider an observed sequence $(\mathbf{C}^o, \mathbf{T}^o)$ and the corresponding thicknesses \mathbf{Z}^o . Here,
 238 the reference to the site is dropped for the sake of clearer notations. Recall that since
 239 the sequence \mathbf{C}^o must be compatible with the parent sequence \mathbf{C} , \mathbf{C}^o is obtained by
 240 deleting some layers of \mathbf{C} .

241 Table 1 shows an example of a parent sequence \mathbf{C} with three categories: Blue, Red
 242 and Green. The observed sequence \mathbf{C}^o is incomplete. Several augmented sequences
 243 \mathbf{C}^a with corresponding depths \mathbf{T}^a are possible. Since in the observed series the first
 244 Blue is followed by Red, the sub-sequence [Blue-Red] must correspond to the
 245 beginning of the parent sequence. Regarding the second occurrence of Blue, three
 246 cases can be distinguished: (i) it corresponds only to the third layer of \mathbf{C} with 4th and
 247 5th layers having null thickness; (ii) it corresponds only to the fifth layer, in which
 248 case the 3rd and 4th layers have null thickness; (iii) it corresponds partly to the 3rd
 249 and partly to the 5th layers. Then, only the 4th layer has 0 thickness. In this last case,
 250 an intermediate, latent, transition at depth \tilde{T} with $T_2^o \leq \tilde{T} \leq T_3^o$ must be introduced.
 251 These augmented series are all possible, but some will be more likely than others,
 252 depending on the parameters of the model. In ‘‘Appendix A’’ an even more complex
 253 example is provided. Only some of the possible configurations are shown. They are
 254 too numerous and complex to be completely listed, even for short parent sequences.

255 In order to estimate the parameters of the model, a data augmentation algorithm
 256 (Tanner 1996, Ch. 5) can be exploited where the complete sequences that are compat-
 257 ible with the observed ones are explored. A Bayesian approach will be adopted for
 258 the inference of the parameters and a Markov Chain Monte Carlo (MCMC) algorithm
 259 will be designed in Sect. 4. But first, a simulation in which all parameters are known
 260 and all sequences are complete is shown.

261 3.4 Simulation

262 Unconditional simulation is straightforward when the transformation φ_j and the
 263 parameters θ_j , $j = 1, \dots, M$, are known. All that is required is to simulate M

Table 1 Example of a parent sequence C with an observed sequence C^o and several possible augmented sequences with corresponding transition depths and thicknesses

Parent C	Observed		Possible augmented sequences								
	C^o	T^o	C^a	T^a	Z^a	C^a	T^a	Z^a	C^a	T^a	Z^a
Blue	Blue	T_1^o	Blue	T_1^o	T_1^o	Blue	T_1^o	T_1^o	Blue	T_1^o	T_1^o
Red	Red	T_2^o	Red	T_2^o	$T_2^o - T_1^o$	Red	T_2^o	$T_2^o - T_1^o$	Red	T_2^o	$T_2^o - T_1^o$
Blue	Blue	T_3^o	Blue	T_3^o	$T_3^o - T_2^o$	Blue	T_2^o	0	Red	\tilde{T}	$\tilde{T} - T_2^o$
Green	-	-		T_3^o	0		T_2^o	0		\tilde{T}	0
Blue	-	-		T_3^o	0	Blue	T_3^o	$T_3^o - T_2^o$	Blue	T_3^o	$T_3^o - \tilde{T}$

Table 2 Parameters for the simulation example

	Black	Red	Blue	Green
μ, β	1	1	1	1
p	0.3	0.8	0.3	0.8
α	20	20	10	10

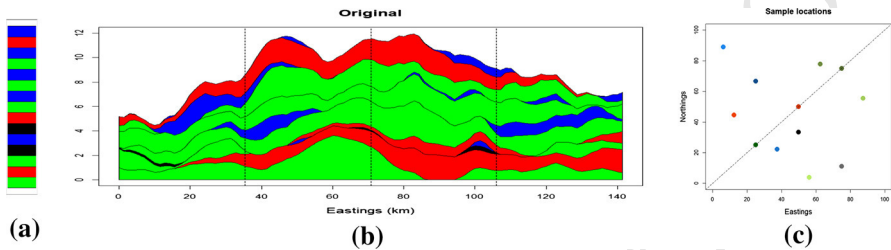


Fig. 2 Simulation experiment: **a** parent sequence of length 15, with 4 lithofacies {Black-Red-Blue-Green}; **b** cross-section of a two-dimensional simulation along the diagonal of $\mathcal{S} = [0, 100] \times [0, 100]$. See Table 2 for the parameters; **c** locations of the twelve boreholes

264 random fields $W_j, j = 1 \dots, M$ and then to apply (1) in order to transform the
 265 Gaussian process into a thickness surface. Figure 2 illustrates a cross-section of
 266 a two-dimensional simulation over $\mathcal{S} = [0, 100] \times [0, 100]$ with four lithofacies
 267 {Black-Red-Blue-Green} and $\varphi_j(x) = \mu_j x$, that is $\beta_j = 1$ for all categories.
 268 The parent sequence has 15 layers (see Fig. 2a) and stochastic models for layers with
 269 the same lithofacies have identical parameters. Thicknesses have been simulated using
 270 Gaussian random fields with a Matérn covariance function

$$271 \quad \rho(h; \nu, \alpha, \sigma^2) = \frac{\sigma^2}{2^{\nu-1} \Gamma(\nu)} \left(\frac{\|h\|}{\alpha} \right)^\nu K_\nu \left(\frac{\|h\|}{\alpha} \right), \quad h \in \mathbb{R}^2, \quad (12)$$

272 where $\nu > 0$ is a smoothness parameter, $\alpha > 0$ a range parameter and σ^2 the sill. Γ
 273 is the gamma function and K_ν is the modified Bessel function of the second kind of
 274 order ν . Here, the smoothness parameter has been set to $\nu = 3/2$ and $\sigma^2 = 1$, which
 275 leads to the simplified expression $\rho_j(h; \alpha_j) = (1 + \|h\|/\alpha_j) \exp(-\|h\|/\alpha_j)$, where
 276 α_j is a range parameter. The set of the parameters in the simulation experiment is
 277 shown in Table 2.

278 twelve synthetic boreholes have been located in \mathcal{S} . Three of them are placed along
 279 the diagonal at coordinates (25, 25), (50,50) and (75, 75). Nine others are randomly
 280 located (see Fig. 2c). For each category, the observed frequencies along these twelve
 281 boreholes are (0.58, 0.83, 0.28, 0.80). Notice that Black is highly over-represented.
 282 The average thicknesses computed along the boreholes are (0.31, 1.31, 0.62, 1.25)
 283 for each of the four categories, whilst the theoretical expectations of each category
 284 computed as per (2) are respectively (1.8, 1.1, 1.8, 1.1). Note here that Black and
 285 Blue are very unlikely to be directly stacked above each other, while it is often the
 286 case for Red and Green.

287 Conditional simulation is relatively easy to implement when the parameters are
 288 known and when complete sequences of thicknesses are available, including all null
 289 thicknesses. Care must be taken when simulating values from the Gaussian distribution
 290 that are below the thresholds τ_j , but otherwise the algorithm, shown in Algorithm 1, is
 291 rather straightforward. Simulations of the truncated Gaussian values are done by call-
 292 ing the function `rmvnorm` of the R package `mvtnorm` (Genz et al. 2019). The reader
 293 is referred to Chilès and Delfiner (2012) for a general exposition on unconditional
 294 simulations and conditional simulations using Kriging techniques.

Algorithm 1 Conditional simulation when all sequences and all parameters are known

Require: Data with complete sequences; transform functions $\varphi_j, j = 1, \dots, M$

Require: All parameters

- 1: **for** $j = 1$ to M **do**
 - 2: Compute the vector $\mathbf{W}_{n_j} = (W_{j,1}, \dots, W_{j,n_j})$ where $W_{j,k} = \varphi_j^{-1}(Z_{j,k})$ corresponding to $Z_{j,k} > 0, k = 1, \dots, n_j$
 - 3: Compute \mathbf{m}_j and \mathbf{V}_j according to (8)
 - 4: Draw a vector of length ℓ_j from a truncated multivariate Gaussian distribution, $\mathbf{W}_{\ell_j} \sim \mathcal{TN}_{\ell_j}(\mathbf{m}_j, \mathbf{V}_j; -\infty, \tau_j)$, for which each component must be below τ_j .
 - 5: Set $\mathbf{W}_j = (\mathbf{W}_{n_j}, \mathbf{W}_{\ell_j})$
 - 6: Simulate a Gaussian random field F_j conditionally on \mathbf{W}_j
 - 7: Transform the field F_j into the thicknesses according to (1)
 - 8: **end for**
-

295 4 Bayesian Inference with a Markov Chain Monte Carlo Algorithm

296 4.1 Sampling All Possible Configurations

297 In order to sample within all possible configurations of the augmented sequence at a
 298 given site s_i that are compatible with the parent sequence, the Markov Chain Monte
 299 Carlo (MCMC) algorithm must be able to delete a layer, to add a new layer or to
 300 displace the limit between two layers of the same category. Recall that the limit between
 301 two different categories are hard conditioning data that cannot be changed. These
 302 elementary moves, illustrated in Fig. 3, are now detailed.

303 *Split:* A state is split into two successive states of the same category. A split is only
 304 possible if it is compatible within the parent sequence. For example, in Fig. 3, the
 305 Blue layer at the bottom can be split into two layers since the parent sequence
 306 contains a second Blue layer. In Table 5 the situation in panel 4 can be obtained
 307 by splitting the state Red, either in panel 2 or in panel 3. When a state is split, a
 308 new transition depth, denoted t_i in Table 5, must be introduced. The thickness is
 309 split in two thicknesses accordingly.

310 *Merge:* This move is the opposite move of *Split*. Two successive states in the
 311 same category are merged together. The corresponding depth is removed and the
 312 resulting thickness is the sum of the two merged thicknesses.

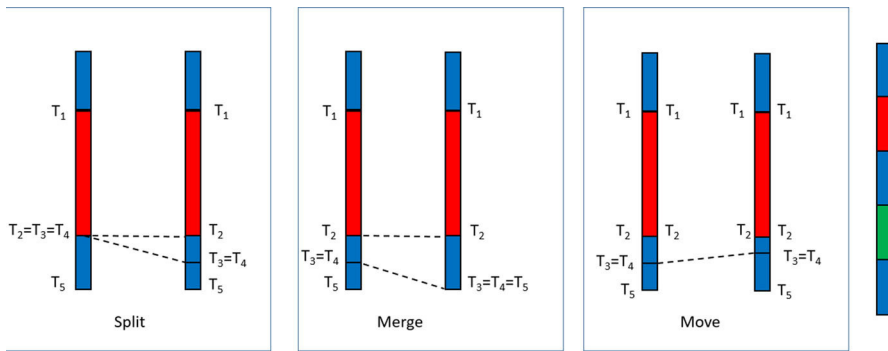


Fig. 3 Elementary moves in an incomplete observed sequence. Note that the layer Green is unobserved. From left to right: *Split*, *Merge* and *Displace*

313 *Displace*: Here, the augmented sequence is not changed, but the intermediate value
 314 between two successive states of the same category is changed. The corresponding
 315 thicknesses are then updated.

316 It is easy to verify that, starting from any initial configuration that is compatible
 317 with the parent sequence, any other configuration can be reached by combining finite
 318 numbers of *Split*, *Merge* and *Displace*. Hence, if these moves are used as building
 319 blocks of a MCMC algorithm, the resulting Markov Chain will be ergodic. At each
 320 borehole, one of the three moves is proposed with probabilities (p_S, p_M, p_D) with
 321 $p_S + p_M + p_D = 1$. If the move is possible, it is accepted according to Metropolis-
 322 Hastings acceptance ratio described in Sect. 4.3.

323 4.2 Choosing the Priors

324 Priors must be defined for all parameters of the model. For the parameters of the
 325 transform functions φ_j , $1 - p_j = \Phi(\tau_j)$ and β_j , uninformative flat priors have been
 326 chosen on the intervals $(0, 1)$ and $(0.25, 4)$, respectively. Regarding the covariance
 327 function, the Matérn covariance function in (12) has been chosen for its great flexibility
 328 thanks to three parameters: $\xi = (\nu, \alpha, \sigma)$, for smoothness, range and sill, respectively.

329 However, it is known that the joint estimation of these parameters is difficult in a
 330 Bayesian context, in particular if the number of data is small. Zhang (2004) showed
 331 that for a Matérn covariance function the only quantity that can be estimated consis-
 332 tently under in-fill asymptotics is $\sigma^2 \alpha^{-2\nu}$. As a consequence, since the parameter μ^2
 333 behaves as the marginal variance of the random field, using uninformative flat priors
 334 for (μ, α, ν) is expected to provide poor posterior distributions for these parameters.
 335 This was indeed confirmed on preliminary MCMC runs (results not reported here).
 336 It was thus decided to fix the smoothness parameter ν among the values $(1/2, 3/2,$
 337 $5/2)$ that would provide the highest likelihood. The above values correspond to covari-
 338 ance functions being the product of an exponential and a polynomial of order p with
 339 $p = 0, 1, 2$ respectively, namely $\rho(r; 1/2, \alpha, 1) = \exp(-r/\alpha)$, $\rho(r; 3/2, \alpha, 1) =$
 340 $(1 + r/\alpha) \exp(-r/\alpha)$ and $\rho(r; 5/2, \alpha, 1) = (1 + r/\alpha + r^2/(3\alpha^2)) \exp(-r/\alpha)$.

341 Simpson et al. (2017) proposed an approach for building priors that are based on
 342 penalizing the complexity to a base model. For example, a random effect with positive
 343 variance is an extension (a more complex version) of random effect with null variance.
 344 Similarly, a random field with a finite range is an extension (a more complex version)
 345 of a random field with an infinite range. Indeed, if the range is infinite, the random
 346 field is perfectly correlated and its spatial variance is null. Penalized Complexity (PC)
 347 priors are then defined as the only priors that: (i) use the Kullback–Leibler divergence
 348 as a measure between the extended and the base models; (ii) have a penalization that
 349 increases with the distance at a constant rate.

350 Fuglstad et al. (2019) derived the PC priors for a Matérn covariance with parameters
 351 σ , α and ν , when ν is fixed. They showed that the joint PC prior corresponding to a
 352 base model with infinite range and zero variance when $d = 2$ is

$$353 \quad \pi(\sigma, \alpha) = \lambda_\alpha \alpha^{-2} \exp(-\lambda_\alpha / \alpha) \lambda_\sigma \exp(-\lambda_\sigma \sigma), \quad (13)$$

354 where $\lambda_\alpha = -\ln(\epsilon_\alpha) / \alpha_0$ and $\lambda_\sigma = -\ln(\epsilon_\sigma) / \sigma_0$, and the values of λ_α and λ_σ are such
 355 that $P(\alpha < \alpha_0) = \epsilon_\alpha$ and $P(\sigma > \sigma_0) = \epsilon_\sigma$. By choosing small probabilities ϵ_α and
 356 ϵ_σ , the range is lower-bounded above α_0 and the standard deviation is upper bounded
 357 at σ_0 with probability $1 - \epsilon_\alpha$ and $1 - \epsilon_\sigma$, respectively. PC priors described in (13)
 358 will be used throughout, where μ plays the role of the standard deviation as shown in
 359 Eq. (3) in Sect. 3.1.

360 4.3 General Description of the Algorithm

361 Each parameter in each category is updated iteratively in a Metropolis-within-Gibbs
 362 algorithm (Gelfand 2000). A new value is proposed according to symmetric transition
 363 kernels, for which it is equally likely to move from a current value y^c to a new value y^n
 364 than the opposite. Let θ^c and θ^n be the current and the proposed vector of parameters
 365 θ , respectively. Let further $\pi(\cdot)$ be the prior density of θ . The acceptance ratio is then

$$366 \quad A(\theta^c, \theta^n) = \frac{L(\theta^n; \mathbf{X})\pi(\theta^n)}{L(\theta^c; \mathbf{X})\pi(\theta^c)}. \quad (14)$$

367 When sampling the configurations thanks to one of the possible moves *Split*, *Merge*
 368 and *Displace*, a new configuration \mathbf{X}^n is proposed, \mathbf{X}^c being the current one. In this
 369 case, the acceptance ratio is

$$370 \quad A(\mathbf{X}^c, \mathbf{X}^n) = \frac{L(\theta; \mathbf{X}^n)}{L(\theta; \mathbf{X}^c)}. \quad (15)$$

371 The proposals are accepted if the acceptance ratios $A(\cdot, \cdot)$ are larger than one. Other-
 372 wise, they are accepted with a probability equal to the ratio. The proposal in the
 373 Metropolis-Hasting step are random walk proposals aiming at an acceptance rate
 374 above 0.5. For sampling new configurations at each borehole in turn, a possible move
 375 is drawn according to the probabilities $p_S = p_M = p_D = 1/3$. Then, it is checked

376 whether such a move is feasible within this borehole. If several moves are possi-
 377 ble, one is selected uniformly among all possible moves in that borehole, and a new
 378 configuration is proposed. The whole procedure is summarized in Algorithm 2.

Algorithm 2 MCMC procedure

Require: Data; parent sequence; transform functions φ_j , $j = 1, \dots, M$

Require: Initial values and priors for all parameters

Require: Number of iterations, N

```

1: for  $i = 1$  to  $N$  do
2:   for each parameter  $\eta \in \{p, \mu, \beta, \alpha\}$  do
3:     for  $j = 1$  to  $M$  do
4:       Propose new  $\eta_j$  according to transition kernel
5:       Compute acceptance ratio,  $A$  using (14)
6:       Generate  $U \sim \mathcal{U}[0, 1]$ ; accept new  $\eta_j$  if ( $U \leq A$ )
7:     end for
8:   end for
9:   for Borehole  $k = 1$  to  $n$  do
10:    Draw a move  $\in \{Split, Merge, Displace\}$  according to the probabilities ( $p_S, p_M, p_D$ )
11:    Check for feasibility within borehole  $k$ 
12:    if (move is feasible) then
13:      Draw uniformly one among all possible moves
14:      Compute acceptance ratio,  $A$  using (15)
15:      Generate  $U \sim \mathcal{U}[0, 1]$ ; accept the move if ( $U \leq A$ )
16:    end if
17:  end for
18: end for

```

379 5 A Synthetic Data Example

380 The MCMC algorithm described above is first validated on the synthetic data-set
 381 described in Sect. 3.4 and illustrated in Fig. 2. It was coded in R using standard
 382 functions and our own code for the *Split*, *Merge* and *Displace* movements. Most of the
 383 running time is spent in computing the simultaneous probabilities of being below 0 in
 384 (7). This is done by calling the function `pmvnorm` of the R package *mvtnorm* (Genz
 385 et al. 2019; Genz and Bretz 2009). Uniform priors are used for the parameters p_j and
 386 β_j , respectively on (0, 1) and (0.25, 4), while PC priors are used for the parameters
 387 μ_j and α_j , as described in details in Sect. 4.2. Here, the setting was $\epsilon_\alpha = \epsilon_\mu = 0.01$,
 388 with $\alpha_0 = 3$ and $\mu_0 = 10$. Algorithm 2 is run for 30,000 iterations, after a burn-in
 389 period of 2,500 iterations. Values of parameters are then sampled every 50 iterations.
 390 The proposals in the Metropolis-Hasting steps follow a uniform random walk with
 391 increments in $[-0.4, 0.4]$ for μ_j and β_j , in $[-0.15, 0.15]$ for p_j and in $[-3, 3]$ for the
 392 range α_j . With these choices, the observed acceptance ratio lies between 0.43 and 0.57,
 393 depending on the parameters. This dataset being quite constrained, the acceptance ratio
 394 for exploring new configurations is only $6.78 \cdot 10^{-5}$.

Fig. 4 Complete log-likelihood as a function of iterations. The log-likelihood values are depicted every 50 iterations

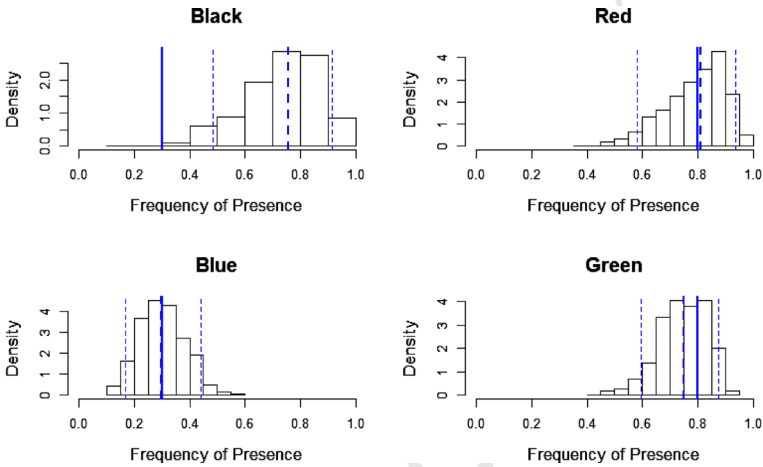
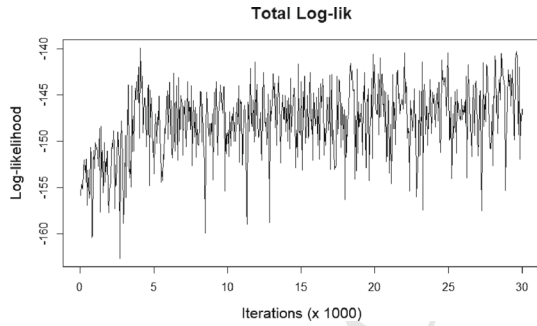


Fig. 5 Posterior histograms of the frequencies p_j . Thick continuous line: true value of the parameter. Dashed thick line: posterior median. Dashed thin lines: posterior 0.05 and 0.95 quantiles

5.1 Estimation of the Parameters

Figure 4 shows the complete log-likelihood as a function of the iterations. The mixing of the Markov chain is satisfactory and MCMC achieves convergence quite quickly. Figure 5 shows the posterior distribution of the frequency of each category. With the exception of the Black category, which was over-represented as already mentioned, the parameters p_j are very well estimated. Figure 6 shows the posterior cross-plot of the parameters β_j (resp. α_j) versus μ_j . One can see that there is some amount of negative correlation between β_j and μ_j , while there is some positive correlation between α_j and μ_j . These findings are quite consistent with the parametric form of the function $\varphi(x) = \mu x^\beta$ on the one hand, and with the result obtained in Zhang (2004) regarding the simultaneous estimation of the range and variance of a Matérn random field on the other hand. One can observe that the posterior median is quite close to the true value and always within the 90% posterior credibility interval, at the exception of the range parameter for the Black category. For this category, it should be remembered that the observed frequency was over-represented (0.58, as compared to 0.3) and that

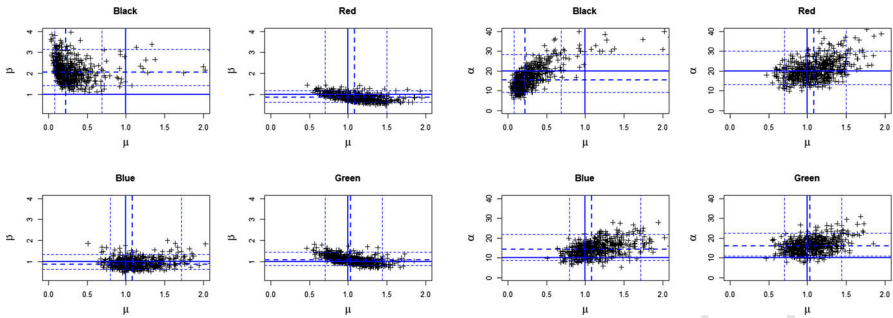


Fig. 6 Left: posterior cross-plot of β_j versus μ_j . Right: posterior cross-plot of α_j versus μ_j . Thick continuous line: true value of the parameter; dashed thick line: posterior medians; dashed thin lines: posterior 0.05 and 0.95 quantiles

410 the average thickness was 0.31 as compared to the theoretical expectation equal to
 411 1.8. The maximum likelihood for the parameters (p_j, μ_j, β_j) is thus completely off
 412 the real values (0.3, 1, 1) as can also be seen on Fig. 6, where μ_j is under-estimated
 413 and β_j is over-estimated (Fig. 6). Nonetheless, given the good performances in the
 414 other categories, these results are quite promising considering that there are only 2 to
 415 5 layers per category and that there are only 12 synthetic boreholes.

416 5.2 Reconstruction of the Sequences

417 The observed sequence is not complete on most boreholes. Augmented sequences
 418 are created during the MCMC iterations. Since they can change along the iterations,
 419 the MCMC algorithm allows us to explore different consistent reconstructions. Fig-
 420 ure 7 shows the thickness of the 15 layers as a function of iterations for the first
 421 six synthetic boreholes. Each layer is color-coded according to its category. Simi-
 422 lar plots were obtained for the other boreholes, but they are not shown here for
 423 the sake of concision. Firstly, it should be noted that the thicknesses do not vary
 424 often and that the variability of the thicknesses is quite different among the layers
 425 and among the boreholes. Red layers show constant thickness because, in the par-
 426 ent sequence, Red layers are separated by 4, respectively 6 layers (see Fig. 2). As a
 427 consequence, the conditioning makes it impossible to *Merge* or *Split* any Red lay-
 428 ers. The relative low number of moves is due to the lateral correlations implied by
 429 the smoothness parameter being equal to $3/2$ and the range parameter being approx-
 430 imately equal to $1/3$ of the size of the domain. On boreholes #1 and #6, there is no
 431 Black layer at all. The variations are not numerous and they concern mostly the
 432 6-layer sequence [Green-Blue-Green-Blue-Green-Blue] that allows some
 433 exchanges of depth through successive moves. In particular, in boreholes #1 and #3
 434 the actual sequence is [Green-Blue-Green-Blue], so that some of the Green
 435 thickness can be exchanged between layers. Note that the total amount of Green
 436 thickness remains always constant. On boreholes #2 to #5, some Black layers are
 437 visible. The parent sequence is [Black-Blue-Black], but on borehole #4 one of
 438 the observed thickness of Blue is 0. As a consequence, the observed Black thick-

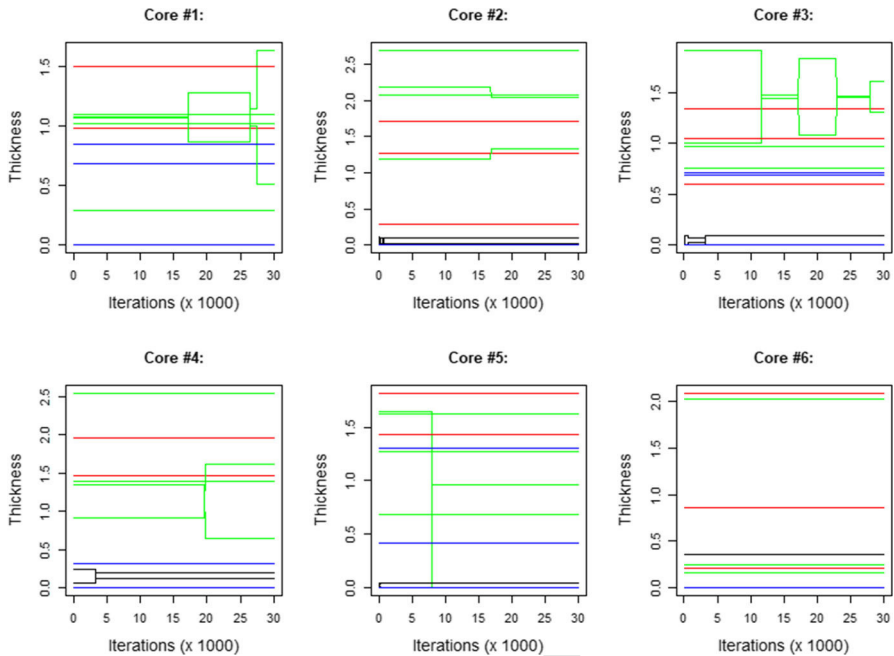


Fig. 7 Thickness of different layers in synthetic boreholes #1 to #6 as a function of iterations. Layers are represented according to the color of the category they belong to

ness can be shared between the two layers, or it can be attributed to one layer only, the other one being zero.

Figure 8 shows the thickness of layers #6 to #11 as a function of iterations for each borehole intersecting the layer. It is the dual representation of Fig. 7. Some layers have constant thickness across all boreholes, as it is the case for the Red layer #7, which intersects 9 out of the 12 boreholes. On the three others, the conditioning does not make it possible to *Merge* or *Split* the layer. In layers #10 and #12, the situation is quite the opposite. Since the total thickness must remain constant, variations on layers #10 and #12 are complementary for Green. These layers are part of the [Green-Blue-Green-Blue] sequence from layer 10 to layer 13 already mentioned. This representation offers a complementary view of the variations of this layer.

5.3 Conditional Simulations

Two ingredients are necessary in order to perform a simulation conditional on the observed data. First, one needs all observed sequences to be coherently completed in accordance with the parent sequence. Second, the simulation requires parameters for μ , β , p and α . These must be jointly sampled from the posterior distribution in a coherent way. Independent and identically distributed sets of augmented sequences and estimated parameters are accessible by sampling from independently MCMC runs after the burn-in period. Alternatively, one can sample from the same MCMC run if the number of iterations between two samples is large enough. The exact number

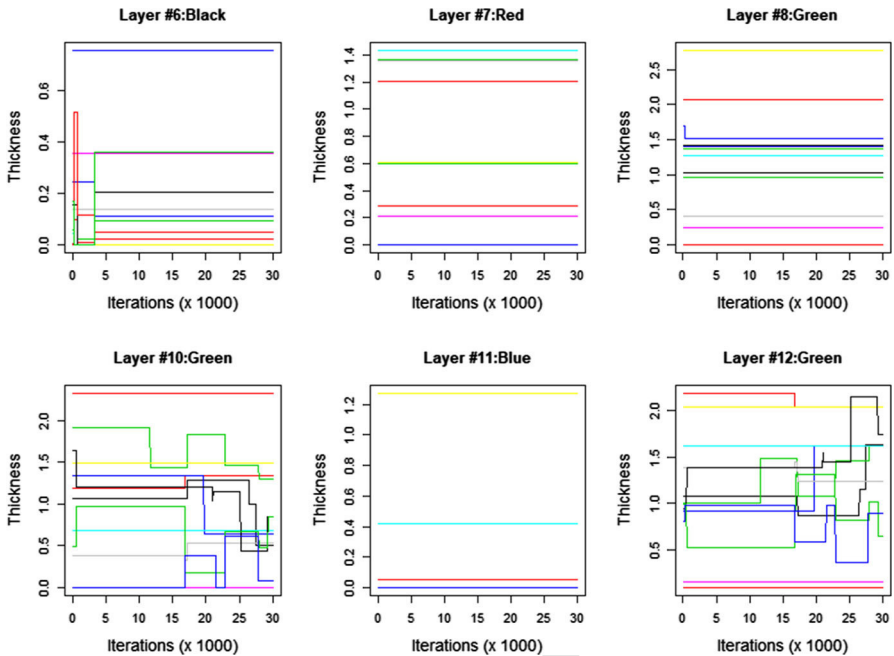


Fig. 8 Thickness of layers #6 to #12 as a function of iterations. Each borehole is represented with a different color

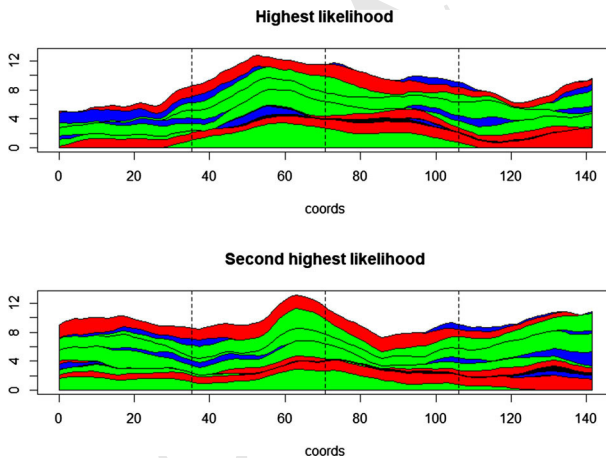


Fig. 9 Two conditional simulations. The completed sequences and the posterior parameters correspond to the most likely configuration of the MCMC run

459 depends on the mixing properties of the MCMC algorithm. In practice, allowing a
 460 number of iterations larger than the burn-in period is a safe enough option. The set
 461 of parameters, together with the completed sequences corresponding to the highest
 462 likelihoods recorded, have been selected for conditional simulations. They are depicted
 463 in Fig. 9. Both simulations honor perfectly the data at the boreholes (dashed vertical

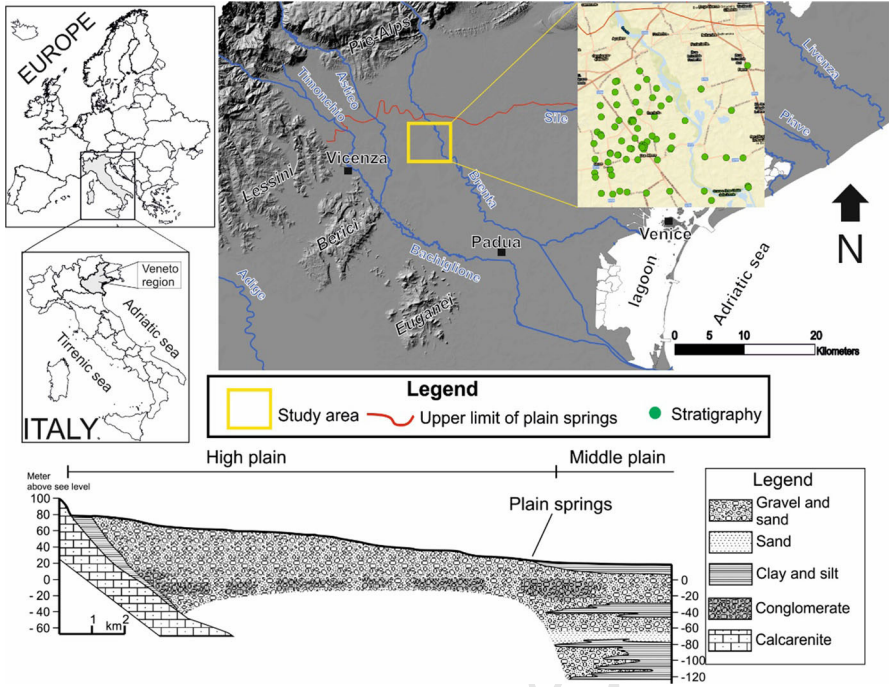


Fig. 10 The study area of the real data example and the stratigraphy

464 lines), but they show significantly different behaviors away from the conditioning
 465 data.

466 **6 A Case Study: Deposition of Materials on an Aquifer**

467 **6.1 Study Area and Dataset Description**

468 The study area (Fig. 10) is in the central part of the Venetian Plain (Italy), on the
 469 Brenta megafan (principally on the right bank of the actual Brenta River) of the North-
 470 ern Padua district. In such an area, several rivers (Bacchiglione, Brenta, Astico and
 471 Timonchio) are responsible for the deposition of a significant portion of the material,
 472 hundreds of meters thick, which forms the subsoil of the Venetian Plain. Along the
 473 piedmont belt of the plain, fans from adjacent rivers laterally penetrate gravelly allu-
 474 vial fans. The result is entirely gravelly subsoil throughout the thickness of the high
 475 Venetian Plain. Because deeper fans often invade further areas of the high plain from
 476 the undifferentiated gravel cover, the terminal parts of the fans extend downstream for
 477 various distances, producing an alluvial cover that is no longer uniformly gravelly, but
 478 is instead composed by alternating layers of gravel and silty clay of swampy, lagoon
 479 or marine origin (Fabbri et al. 2016).

480 The data-set contains 24 boreholes drilled in a 5 km × 6 km region, with a minimum
 481 distance between boreholes of 0.23 km (Fig. 11, top-left panel). Since the maximum

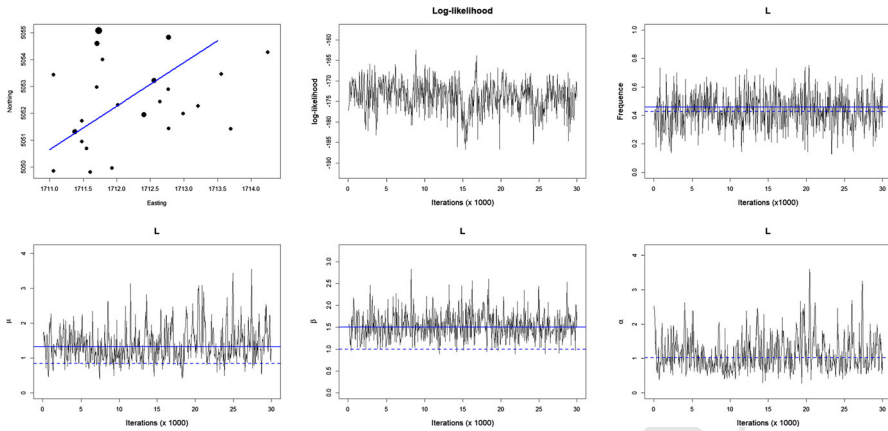


Fig. 11 Location of the 24 boreholes analyzed in the Veneto dataset (top left); diameter is proportional to the number of thicknesses recorded (from 2 to 4); thick blue line: cross-section for conditional simulation. Then, from top to bottom and from left to right: total likelihood, p , μ , β and α as a function of iterations for category L. Continuous lines: posterior medians. Dashed lines: initial values

Table 3 Empirical estimates of presence, average thickness and initial values for τ and μ

	L	S	G	A	Overall
Number of records	22	18	12	3	55
Proportion of presence, $p_j(0)$	0.46	0.75	0.25	0.13	0.38
Average thickness (in m), \bar{T}_j	0.73	2.25	3.89	1.10	1.94
Initial value, $\tau_j(0)$	0.10	-0.67	0.67	1.15	—
initial value, $\mu_j(0)$	0.96	2.06	6.52	2.21	—

482 depth of the boreholes is highly variable, a depth window between the surface (from
 483 35 m to 40 m above sea level) and 25 m above sea level is selected. There are four
 484 categories L(imo) (Silt), S(abbia) (Sand), G(hiaia) (Gravel), A(rgilla) (Clay) and the
 485 parent sequence, containing six layers, is: [L-S-G-L-A-G]. Notice that, since there
 486 is only one layer for S and A, the associated thicknesses on the boreholes are known
 487 without ambiguity when present, which is not necessarily the case for the thicknesses
 488 associated to L and G. From two to four layers are observed on each borehole. One
 489 borehole contains an observed sequence of length 4 and five boreholes contain an
 490 observed sequence of length 3. The empirical estimates of the presence and the average
 491 thicknesses are shown in Table 3. The most observed categories are S followed by L
 492 as measured by the proportion of presence (for L, $\rho_j(0) = 22/(2 \times 24) = 0.46$. The
 493 less observed category is A, with three records only.

494 6.2 Model Setting

495 The empirical estimates are transformed into initial values for τ_j and μ_j , by setting
 496 initial values for β_j to $\beta_j(0) = 1$. Thus, for each category j

$$\mu_j(0) = \frac{\bar{T}_j p_j(0)}{\phi(\tau_j(0))}, \quad \text{with } \tau_j(0) = \Phi^{-1}(1 - p_j(0)).$$

Preliminary tests (not reported here) showed that the likelihood computed with a Matérn covariance function is almost always significantly larger with a smoothness parameter $\nu = 1/2$ than with $\nu = 3/2$ or $\nu = 5/2$. Therefore, the parameter ν is set to $1/2$, corresponding to an exponential covariance function, even though this covariance function corresponds to continuous but non differentiable random surfaces. This point will be further discussed in Sect. 7. Initial values for the range are set to 1 km.

In this dataset, sequences are highly incomplete. As a consequence, the MCMC algorithm needs to have good mixing properties in order to explore the many possible augmented sequences that are compatible with the observations. Proposals follow a random walk with flat uninformative priors similar to that of Sect. 4 for p_j and β_j . PC priors were used for μ_j and α_j , with $\epsilon_\alpha = \epsilon_\mu = 0.01$ and $(\alpha_0, \mu_0) = (0.25, 10)$. Algorithm 2 is run for 30,000 iterations, after a burn-in period of 2,500 iterations. The values of the parameters are then sampled every 50 iterations, so that $m = 600$ posterior samples are collected. The proposals in the Metropolis-Hasting steps follow a uniform random walk with increments in $[-0.4, 0.4]$ for μ_j and β_j , in $[-0.15, 0.15]$ for p_j and in $[-0.2, 0.2]$ for the range α_j . With these choices, the acceptance ratio for the parameters was around 0.8. Although it is higher than recommended, it does not appear to have a negative impact on the estimation procedure. Instead the acceptance ratio of new thickness configurations was equal to 0.22 due to the incompleteness of this data set. Figure 11 shows the values of the parameters p , μ , β and α as a function of iterations after burn-in, for category L. It is quite clear that the chain is stationary with good mixing. Notice the difference between the initial values and the posterior medians. Similar results have been obtained for the other categories.

6.3 Results

6.3.1 Analysis of Thicknesses

When data belonging to the categories L and G are observed on the boreholes, the recorded thickness might belong to a single layer or to two layers. For these categories, the posterior thickness distribution might therefore look different from the observed one. Figure 12 (left) shows how thicknesses of the first layer L in borehole #1 vary along iterations thanks to the *Split*, *Merge* and *Displace* moves of the MCMC. On this borehole, the observed sequence is [L-A-G]. The measured thickness for L is equal to 0.4. Since the parent sequence is [L-S-G-L-A-G] this thickness could correspond to the first layer only (case I), to the fourth layer only (case II), or it could be shared between the two layers (case III). Figure 12 (right) represents the posterior histogram of the thickness in the first layer. Case I corresponds to 0.4, case II to 0 and case III to any value in the interval $(0, 0.4)$. Frequencies computed along the iterations reveal that case III is the most likely case, with an estimated probability of 0.47. The probabilities of case I and case II are equal to 0.42 and 0.11, respectively. A similar analysis can be performed easily on other boreholes and categories.

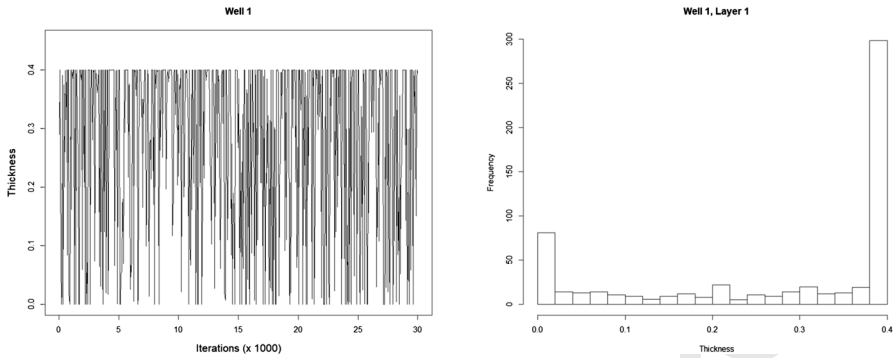


Fig. 12 Thickness of the first layer L in borehole # 1. Left: as a function of iterations. Right: posterior histogram

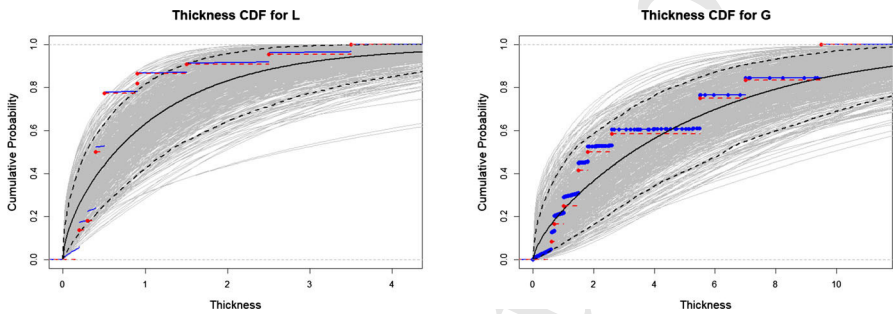


Fig. 13 Thickness cumulative distributions (TCD). In gray: MCMC samples of the posterior theoretical TCD according to (16); black continuous curve: pointwise posterior median TCD; black dashed curves: pointwise posterior 0.05 and 0.95 posterior quantiles. Red dashed curve: TCD of the original data; blue curve: TCD of the MCMC samples. Left: category L ; right: category G

537 For a given category (for simplicity the index j is dropped), and for given parameters
 538 (p, μ, β) , the theoretical thickness cumulative distribution (TCD) is

$$539 \quad P(Z \leq z \mid p, \mu, \beta) = \int_{\tau}^{\tau+(z/\mu)^{1/\beta}} \frac{\phi(y)}{p} dy = \frac{\Phi(\tau + (z/\mu)^{1/\beta}) - \Phi(\tau)}{p}, \quad (16)$$

540 with $\Phi(\tau) = 1 - p$. The parameters are sampled every 50 iterations of the MCMC,
 541 thereby mitigating the correlation between successive samples. At each recorded iteration
 542 $k = 1, \dots, m$, the posterior samples $p(k), \mu(k)$ and $\beta(k)$ make it possible to
 543 compute a posterior theoretical TCD according to (16). Those are represented in gray
 544 on Fig. 13 for categories L and G . The ensemble of m posterior TCDs allows us
 545 to compute pointwise median and the pointwise quantiles $q_{0.05}$ and $q_{0.95}$, which are
 546 represented with black continuous and dashed lines, respectively.

547 Empirical posterior TCD can alternatively be computed from the thickness values
 548 recorded along the sampled iterations $k = 1, \dots, m$. In principle, empirical and
 549 theoretical TCDs should match. Figure 13 shows the original and posterior TCDs,
 550 respectively in red and blue. Thanks to the *Split*, *Merge* and *Displace* movements, the

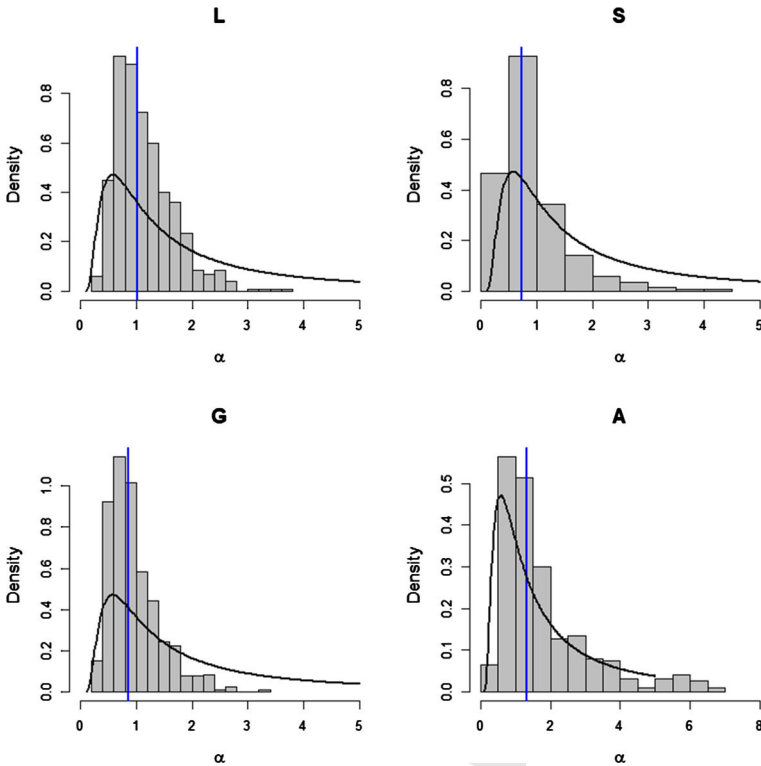


Fig. 14 For each category, posterior histogram of the spatial range and prior distribution (continuous line). Blue vertical line: posterior median

551 posterior TCD is slightly smoother than the original one since values intermediate to
 552 the observed ones are simulated.

553 Overall, the match between the empirical and the theoretical TCD is very satisfac-
 554 tory since the empirical curve is fully included in the envelope of the MCMC samples
 555 for category G and is mostly included in the envelope for category L.

556 *6.3.2 Spatial Analysis and Conditional Simulation*

557 Figure 14 shows the posterior histograms of the spatial range for the four categories,
 558 with the prior density also shown. This figure indicates that the prior has a heavy weight
 559 on the posterior distributions for each unit. However, when a category is well informed
 560 (L and G), the posterior distribution is more concentrated around the posterior median
 561 (indicated with a vertical blue line), equal to 1.03, 0.73 and 0.85 for categories L,
 562 S and G, respectively. On the contrary, category A has only three records. Since the
 563 likelihood contains very little information, the posterior distribution is very close to
 564 the prior one. The result of this analysis is that there is indeed a significant amount of
 565 spatial correlations in the random fields modeling the thickness of the layers for all
 566 categories but A.

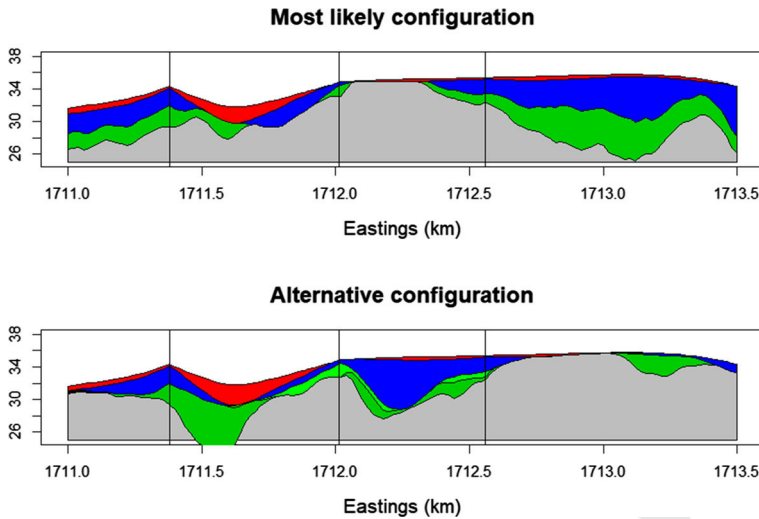


Fig. 15 Two cross-sections along the line shown in Fig. 11 (top left). Notice that there are two different layers for G in the bottom cross-section

567 Figure 15 shows two conditional simulations performed along the cross-section
 568 depicted in Fig. 11 (top left). This cross-section has been chosen because it is close to
 569 three conditioning boreholes (shown with black vertical lines on Fig. 15)
 570 with incomplete observed sequences that allow different thickness configurations in category G.
 571 The color code is the following: red for L, blue for S, green for G and black for A.
 572 The gray color corresponds to undefined lithofacies below the last recorded layer. The
 573 first cross-section corresponds to iteration 8,900 after burn-in, for which the likelihood
 574 was the highest along the whole MCMC (log-likelihood is equal to -162.5). Here,
 575 the G thickness is entirely in layer # 6. The second cross-section corresponds to a
 576 configuration where the G thickness is now shared between the two layers. Different
 577 shades of green have been used to distinguish the two layers. This second configura-
 578 tion corresponds to the most likely configuration with shared thicknesses between
 579 the two G layers (log-likelihood is equal to -171.3). Notice that it is significantly
 580 less likely than the first configuration, indicating that the data is orders of magnitude
 581 less likely with the second configuration than with the first one. Notice also that the
 582 cross-sections are quite different when moving away from the conditioning boreholes.
 583 The parameters corresponding to these two configurations are reported in Table 4.

584 7 Concluding Remarks

585 In this paper a new rule-based approach for simulating depositional sequences of
 586 surfaces conditionally to lithofacies thickness data has been presented. A distinctive
 587 feature of this approach is that it takes into account in a coherent way the different
 588 amount of information along horizontal and vertical dimensions that are usually con-

Table 4 Parameters corresponding to the two configurations shown in Fig. 15

	First configuration Log-likelihood = -162.5				Second configuration Log-likelihood = -171.3			
	L	S	G	A	L	S	G	A
p_j	0.40	0.81	0.23	0.05	0.45	0.64	0.46	0.48
μ_j	1.29	1.80	6.99	2.20	1.98	2.02	5.01	11.03
β_j	1.54	1.59	1.01	0.50	1.42	1.41	1.39	1.76
α_j	1.25	0.29	0.78	0.71	2.03	0.54	0.43	3.58

589 tained in borehole datasets: few cores and, consequently, few horizontal information
590 but complete information along the depth.

591 This is achieved by supposing that there exists a common lithological sequence of
592 facies that is compatible with the observed data. Moreover the sequence is supposed
593 to be known in advance. The facies thickness, which is non-negative, is modeled by
594 means of a truncated and transformed stationary Gaussian field. In principle, other
595 non-negative random fields could be considered, but this choice made it possible to
596 exploit the flexibility of Gaussian random fields in the selection of the covariance
597 functions with different degrees of smoothness. The evaluation of the likelihood is
598 made possible thanks to the Gaussian framework for which well known methods and
599 efficient computing tools are available.

600 A data augmentation algorithm, coupled with a MCMC algorithm, is employed for
601 learning the parameters of the stochastic model from borehole data. A very interesting
602 feature of the proposed algorithm is that the exploration of all different configurations
603 that are compatible with the available data is possible. Thanks to the MCMC approach
604 and the Bayesian framework, it associates a likelihood to each of the possible real-
605 izations corresponding to a set of parameters. From those, as shown in Sect. 6.3, one
606 can assess an empirical probability for each different configuration, select the most
607 likely configurations and compute many other statistics of interest to the user. The
608 algorithm requires multiple (to the order of $M \times n$) evaluations of the joint probability
609 of a Gaussian vector being below a given threshold. The current implementation in R
610 uses the `mvtnorm` package (Genz et al. 2019) that handles vectors with a few dozens
611 of coordinates rather easily. It starts to slow down quite significantly around 100 coord-
612 inates and is unable to cope with more than 1,000 coordinates. Further research is
613 thus required if the number of boreholes goes from moderate to high or very high.
614 One possible choice could be the approximation proposed in Martinetti and Geniaux
615 (2017), but the impact of using a less precise approximation remains to be evaluated.

616 A too small dataset entails difficulties in specifying the regularity and the range of
617 the covariance function, as was shown with category A that has only three records. It
618 was found in the present work that parameters were reasonably well estimated with
619 15 records per category. On the other hand, as the data set gets larger and denser (e.g.
620 when the horizontal distance between nearest neighbor boreholes becomes a small
621 fraction of the range parameter) the likelihood will get more peaked around local
622 maxima, thereby decreasing the mixing of the MCMC. In this case, exploring all

623 configurations coherent with the parent sequence is likely to become more difficult.
624 Longer chains and multiple chains starting from very different initial configurations
625 will probably be necessary.

626 Several assumptions and restrictions have been made in this work, which can be
627 lifted in order to generalize this work. The stationarity assumption, which has proved
628 appropriate here, could be relaxed and the parameters could be easily modified to take
629 covariates into account. Only a few half-integer values of the smoothness parameters
630 have been considered, and the fitting of this parameter was done outside the MCMC
631 machinery. In principle, the smoothness parameter could be different for different
632 facies and it could be estimated in the Bayesian framework, just as any other parameter.
633 Estimating simultaneously the three parameters of the Matérn covariance in a Bayesian
634 context is known to be extremely difficult. When there are only few data, this was
635 made possible thanks to the PC priors (Fuglstad et al. 2019). Currently, to the best
636 of our knowledge, the simultaneous PC prior for (ν, α, σ^2) for Matérn covariance is
637 unknown. Finding such PC priors is left for further research.

638 Currently, independent MCMCs are launched, one for every possible value $\nu \in$
639 $\{1/2, 3/2, 5/2\}$. The one with the highest likelihood and the best mixing is selected
640 and ν is fixed at that value. When analyzing the data from the Venetian plain, it was
641 found that $\nu = 1/2$ was best, despite the fact that the associated thicknesses (and
642 thus surfaces) are mean-square continuous but not differentiable. One could have
643 imposed $\nu = 3/2$, but at the cost of a very short spatial range implying almost no
644 spatial correlation. Whether one should let the data speak or impose a model for the
645 regularity is a debate. Here, a data-driven approach was chosen.

646 Finally, the function that transforms the Gaussian values to thicknesses was chosen
647 to be a power function, but any other positive function could be used.

648 One information that is often available in real applications and on much more points
649 than boreholes is the nature of the facies on the surface. It is possible to incorporate
650 such information at the cost of small changes in the method. At a given location s
651 where this information is available, one could consider that the facies of the upper
652 layer, say facies j , is known and has a positive thickness. The conditioning data would
653 therefore be that $W_{\text{upper}}(x) > \tau_j$. This conditioning can easily be handled within
654 our MCMC procedure. At this location, there would be no conditioning for the other
655 layers.

656 The proposed approach depends on the existence and the knowledge of a common
657 lithological sequence of facies that is compatible with the observed data. If the
658 sequence is unknown, it is possible to derive it from the data, possibly by impos-
659 ing some restriction, such as minimum length. This problem has not been tackled
660 here, since it has been considered beyond the scope of this work. However it is worth
661 mentioning that the approach presented here can be modified to account for several
662 different parent sequences with their associated prior probabilities.

663 **Acknowledgements** This work was initiated during a visit of the first author to Ca' Foscari University of
664 Venice. He acknowledges the support of that institution. We wish to thank two anonymous reviewers for
665 their in-depth and detailed reading of the first version of the manuscript. Their many valuable comments
666 helped us to improve the manuscript.

667 **Appendix A: A Longer Example of Incomplete Sequence**

668 See Table 5.

Table 5 A longer and more complex example of a parent sequence $C=[\text{Blue-Red, Blue-Green-Blue-Red-Green-Blue}]$ with respect to a recorded sequence C^o and T^o

Parent C	Recorded		Compatible augmented sequences								
	C^o	T^o	C^a	T^a	Z^a	C^a	T^a	Z^a	C^a	T^a	Z^a
Blue	Blue	T_1^o	Blue	T_1^o	T_1^o	Blue	T_1^o	T_1^o	Blue	T_1^o	T_1^o
Red	Red	T_2^o	Red	T_2^o	$T_2^o - T_1^o$	Red	T_2^o	$T_2^o - T_1^o$		T_1^o	0
Blue	Green	T_3^o		T_2^o	0		T_2^o	0		T_1^o	0
Green	Blue	T_4^o	Green	T_3^o	$T_3^o - T_2^o$		T_2^o	0		T_1^o	0
Blue	-	-	Blue	T_4^o	$T_4^o - T_3^o$		T_2^o	0		T_1^o	0
Red	-	-		T_4^o	0		T_2^o	0	Red	T_2^o	$T_2^o - T_1^o$
Green	-	-		T_4^o	0	Green	T_3^o	$T_3^o - T_2^o$	Green	T_3^o	$T_3^o - T_2^o$
Blue	-	-		T_4^o	0	Blue	T_4^o	$T_4^o - T_3^o$	Blue	T_4^o	$T_4^o - T_3^o$
			Blue	T_1^o	T_1^o	Blue	T_1^o	T_1^o	Blue	T_1^o	T_1^o
			Red	\tilde{T}	$\tilde{T} - T_1^o$	Red	T_2^o	$T_2^o - T_1^o$		T_1^o	0
				\tilde{T}	0		T_2^o	0	Red	T_2^o	$T_2^o - T_1^o$
				\tilde{T}	0	Green	\tilde{T}	$\tilde{T} - T_2^o$	Green	T_3^o	$T_3^o - T_2^o$
				\tilde{T}	0		\tilde{T}	0	Blue	\tilde{T}	$\tilde{T} - T_3^o$
			Red	T_2^o	$T_2^o - \tilde{T}$		\tilde{T}	0		\tilde{T}	0
			Green	T_3^o	$T_3^o - T_2^o$	Green	T_3^o	$T_3^o - \tilde{T}$		\tilde{T}	0
			Blue	T_4^o	$T_4^o - T_3^o$	Blue	T_4^o	$T_4^o - T_3^o$	Blue	T_4^o	$T_4^o - \tilde{T}$
			Blue	\tilde{T}	\tilde{T}	Blue	\tilde{T}	\tilde{T}	Blue	\tilde{T}	\tilde{T}
				\tilde{T}	0		\tilde{T}	0		\tilde{T}	0
				\tilde{T}	0	Blue	T_1^o	$T_1^o - \tilde{T}$	Blue	$\tilde{\tilde{T}}$	$\tilde{\tilde{T}} - \tilde{T}$
				\tilde{T}	0		T_1^o	0		$\tilde{\tilde{T}}$	0
			Blue	T_1^o	$T_1^o - \tilde{T}$		T_1^o	0	Blue	T_1^o	$T_1^o - \tilde{\tilde{T}}$
			Red	T_2^o	$T_2^o - T_1^o$	Red	T_2^o	$T_2^o - T_1^o$	Red	T_2^o	$T_2^o - T_1^o$
			Green	T_3^o	$T_3^o - T_2^o$	Green	T_3^o	$T_3^o - T_2^o$	Green	T_3^o	$T_3^o - T_2^o$
			Blue	T_4^o	$T_4^o - T_3^o$	Blue	T_4^o	$T_4^o - T_3^o$	Blue	T_4^o	$T_4^o - T_3^o$

Only nine compatible augmented sequences are reported

669 **References**

670 Allard D, Froidevaux R, Biver P (2006) Conditional simulation of multi-type non stationary Markov object
 671 models respecting specified proportions. Math Geol 38(8):959–986
 672 Allard D, D’Or D, Froidevaux R (2011) An efficient maximum entropy approach for categorical variable
 673 prediction. Eur J Soil Sci 62(3):381–393

Author Proof

- 674 Allcroft DJ, Glasbey CA (2003) A latent Gaussian Markov random-field model for spatiotemporal rainfall
675 disaggregation. *J R Stat Soc Ser C Appl Stat* 52(4):487–498
- 676 Armstrong M, Galli A, Beucher H, Loc'h G, Renard D, Doligez B, Eschard R, Geffroy F (2011) Plurigaussian
677 simulations in geosciences. Springer, Berlin
- 678 Baxevani A, Lennartsson J (2015) A spatiotemporal precipitation generator based on a censored latent
679 Gaussian field. *Water Resour Res* 51(6):4338–4358
- 680 Benoit L, Allard D, Mariethoz G (2018a) Stochastic rainfall modeling at sub-kilometer scale. *Water Resour*
681 *Res* 54(6):4108–4130
- 682 Benoit N, Marcotte D, Boucher A, D'Or D, Bajc A, Rezaee H (2018b) Directional hydrostratigraphic units
683 simulation using MCP algorithm. *Stoch Environ Res Risk Assess* 32(5):1435–1455
- 684 Bertonecello A, Sun T, Li H, Mariethoz G, Caers J (2013) Conditioning surface-based geological models to
685 well and thickness data. *Math Geosci* 45(7):873–893
- 686 Beucher H, Galli A, Le Loc'h G, Ravanne C, Group H et al (1993) Including a regional trend in reservoir
687 modelling using the truncated Gaussian method. In: Soares (ed) *Geostat Tróia'92*. Kluwer, pp 555–566
- 688 Carle SF, Fogg GE (1996) Transition probability-based indicator geostatistics. *Math Geol* 28(4):453–476
- 689 Chilès J-P, Delfiner P (2012) *Geostatistics: modeling spatial uncertainty*, 2nd edn. Wiley, New York
- 690 Comunian A, Renard P, Straubhaar J (2012) 3D multiple-point statistics simulation using 2D training
691 images. *Comput Geosci* 40:49–65
- 692 Comunian A, Jha SK, Giambastiani BM, Mariethoz G, Kelly BF (2014) Training images from process-
693 imitating methods. *Math Geosci* 46(2):241–260
- 694 Cressie N (1993). *Statistics for spatial data*, revised edition. Wiley, New York
- 695 Fabbri P, Piccinini L, Marcolongo E, Pola M, Conchetto E, Zangheri P (2016) Does a change of irrigation
696 technique impact on groundwater resources? A case study in Northeastern Italy. *Environ Sci Policy*
697 63:63–75
- 698 Fuglstad G-A, Simpson D, Lindgren F, Rue H (2019) Constructing priors that penalize the complexity of
699 Gaussian random fields. *J Am Stat Assoc* 114(525):445–452
- 700 Galli A, Beucher H, Le Loc'h G, Doligez B, Group H (1994) The pros and cons of the truncated Gaussian
701 method. *Geostatistical simulations*. Springer, Berlin, pp 217–233
- 702 Gelfand AE (2000) Gibbs sampling. *J Am Stat Assoc* 95(452):1300–1304
- 703 Genz A, Bretz F (2009) *Computation of multivariate normal and t probabilities*. Lecture notes in statistics,
704 Springer, Heidelberg
- 705 Genz A, Bretz F, Miwa T, Mi X, Leisch F, Scheipl F, Hothorn T (2019) *mvtnorm: multivariate normal and*
706 *t distributions*. R package version 1.0-11
- 707 Le Blévec T, Dubrule O, John CM, Hampson GJ (2017) Modelling asymmetrical facies successions using
708 pluri-Gaussian simulations. *Geostatistics Valencia 2016*. Springer, Berlin, pp 59–75
- 709 Le Blévec T, Dubrule O, John CM, Hampson GJ (2018) Geostatistical modelling of cyclic and rhythmic
710 facies architectures. *Math Geosci* 50(6):609–637
- 711 Liu L, Shih Y-CT, Strawderman RL, Zhang D, Johnson BA, Chai H et al (2019) Statistical analysis of
712 zero-inflated nonnegative continuous data: a review. *Stat Sci* 34(2):253–279
- 713 Marcotte D, Allard D (2018) Gibbs sampling on large lattice with GMRF. *Comput Geosci* 111:190–199
- 714 Mariethoz G, Caers J (2014) *Multiple-point geostatistics: stochastic modeling with training images*. Wiley,
715 New York
- 716 Martinetti D, Geniaux G (2017) Approximate likelihood estimation of spatial probit models. *Region Sci*
717 *Urban Econ* 64:30–45
- 718 Matheron G, Beucher H, De Fouquet C, Galli A, Guerillot D, Ravanne C et al (1987) Conditional simulation
719 of the geometry of fluvio-deltaic reservoirs. In: SPE annual technical conference and exhibition.
720 Society of Petroleum Engineers
- 721 Pyrcz MJ, Sech RP, Covault JA, Willis BJ, Sylvester Z, Sun T, Garner D (2015) Stratigraphic rule-based
722 reservoir modeling. *Bull Can Pet Geol* 63(4):287–303
- 723 Sartore L, Fabbri P, Gaetan C (2016) spMC: an R-package for 3D lithological reconstructions based on
724 spatial Markov chains. *Comput Geosci* 94:40–47
- 725 Simpson D, Rue H, Hiebler A, Martins TG, Sørbye SH et al (2017) Penalising model component complexity:
726 a principled, practical approach to constructing priors. *Stat Sci* 32(1):1–28
- 727 Strebelle S (2002) Conditional simulation of complex geological structures using multiple-point statistics.
728 *Math Geol* 34(1):1–21
- 729 Syversveen AR, Omre H (1997) Conditioning of marked point processes within a Bayesian framework.
730 *Scand J Stat* 24(3):341–352

- 731 Tanner MA (1996) Tools for statistical inference: methods for the exploration of posterior distributions and
732 likelihood functions. Springer, Berlin
733 Zhang H (2004) Inconsistent estimation and asymptotically equal interpolations in model-based geostatistics. J Am Stat Assoc 99(465):250–261
734

uncorrected proof

Journal: 11004
Article: 9875

Author Query Form

**Please ensure you fill out your response to the queries raised below
and return this form along with your corrections**

Dear Author

During the process of typesetting your article, the following queries have arisen. Please check your typeset proof carefully against the queries listed below and mark the necessary changes either directly on the proof/online grid or in the 'Author's response' area provided below

Query	Details required	Author's response
1.	Please check and confirm if the authors and their respective affiliations have been correctly identified.	
2.	Please confirm if the corresponding author is correctly identified.	